Welding in the World (2023) 67:923–934
https://doi.org/10.1007/s40194-023-01476-9

RESEARCH PAPER

Parametric study of melt pool geometry in hybrid plasma arc-laser melting process for additive manufacturing application

Chong Wang[1] · Wojciech Suder[1] · Jialuo Ding[1] · Stewart Williams[1]

Received: 8 October 2022 / Accepted: 10 January 2023 / Published online: 20 January 2023

Abstract
Wire-based hybrid arc-laser additive manufacturing is suitable for producing large metallic parts (metres in scale) with high deposition rates and near-net-shape. In this process, the surface quality and dimensional accuracy of the deposited parts are determined by the melt pool geometry. However, how to control the melt pool in the hybrid process is complex due to the multiple parameters that can be used. In this study, control of melt pool geometry by investigating different process parameters, including laser power, travel direction, arc-laser separation distance, laser beam size, and arc current in the hybrid plasma transferred arc (PTA)-laser process, was studied systematically. It was found that a larger melt pool was achieved with the PTA-leading configuration compared to that with the laser-leading configuration due to a higher laser absorption occurred with the former configuration. The melt pool was enlarged by either increasing the laser power or arc current due to the increased energy input. However, if the laser power density is high enough to determine the melt pool depth, the increasing arc current has very little effect on melt pool depth but only increases the melt pool width. In addition, the melt pool became shallower and wider when using a larger laser beam. The arc-laser separation distance had a minor effect on the melt pool geometry due to the fixed energy input used in the studied cases. The results of this study provide a reference for melt pool control in wire-based hybrid arc-laser additive manufacturing.

Keywords Hybrid arc-laser additive manufacturing · Plasma transferred arc · Laser · Parametric study · Laser absorption · Melt pool geometry

1 Introduction

Additive manufacturing (AM) has developed rapidly over the last few decades due to its significant benefits, such as short lead-time, low material waste, and high design flexibility, over the traditional subtractive manufacturing methods [1–3]. Depending on the heat source used, there are three main AM processes for metallic components deposition, which are laser-based, electron beam-based, and electric arc-based processes [4–6]. Depending on the form the feedstock used, there are wire-based and powder-based processes [7, 8]. Recently, a wire-based hybrid AM process by combining the advantages of both electric arc (e.g. high efficiency) and laser (e.g. high precision) was proposed to achieve both high deposition rate and high resolution for the deposition of large-scale metallic components [9–11]. It has been reported that compared to the plasma transferred arc (PTA) process on its own, the hybrid process has a higher deposition rate due to the extended energy distribution. Compared to the laser deposition process, the hybrid process has a much higher wire melting efficiency and wire feeding tolerance due to the use of PTA [9]. However, since the hybrid arc-laser AM is a relatively new process, some fundamentals in this process are still not fully understood. For example, control of the melt pool in the hybrid process is of great significance, as the melt pool geometry determines the size and shape of the deposited beads, which affect the final quality of the deposited components. Therefore, it is essential to investigate how to control the melt pool geometry in the hybrid process to achieve structurally sound components.

So far, most studies on hybrid arc-laser process have been focused on welding applications [12–16]. In some

Recommended for publication by Commission I - Additive Manufacturing, Surfacing, and Thermal Cutting.

✉ Chong Wang
chong.wang1@cranfield.ac.uk

[1] Welding and Additive Manufacturing Centre, Cranfield University, Bedfordshire MK43 0AL, Cranfield, UK

respects, same phenomena were observed in both hybrid welding and hybrid AM. For example, the melt pool width and depth are inversely affected by the travel speed in hybrid welding [17–20], which is consistent with that observed in hybrid AM [10]. The reduced melt pool width and depth with the increased travel speed was caused by the reduced line energy. However, due to the different requirements between welding and AM, the optimum operating conditions for hybrid welding could be different from hybrid AM. For example, in hybrid welding, a keyhole regime of the laser is normally used to increase the penetration depth [21]. In AM, however, a high width-to-height aspect ratio of the bead with a low remelting is favourable to achieve a high process efficiency and good surface finish, meaning that a relatively large laser beam in conduction regime is needed [11, 22]. In addition, in some hybrid welding cases, the laser is placed very close to the gas metal arc (GMA) to stabilise the arc and thus to achieve a high process stability [23]. Therefore, to ensure the synergic effect of the arc and laser, the separation distance between the two heat sources is normally kept very close (from 0 to 5 mm) in hybrid welding [12]. In hybrid AM, however, the arc-laser separation distance is relatively long as the synergic effect is not needed. These suggest that a systematic study of melt pool control in the hybrid AM process is necessary although similar studies have been conducted in hybrid welding processes.

In hybrid arc-laser AM, the melt pool is formed by a combined effect of arc and laser, and therefore, it is important to understand how the energy input from the arc and laser affects the melt pool geometry. In addition, the laser beam size can be tuned in the hybrid AM process, which will change the energy distribution and consequently the melt pool geometry. Furthermore, there are two main travel directions (or heat source configurations) that can be used in hybrid AM, which are arc-leading and laser-leading. However, it is still unclear how all these processing conditions affect the melt pool geometry. Wang et al. [11] developed a steady-state FE model to study the melt pool geometry in the hybrid PTA-laser melting process. The effect of different process parameters, including laser power, travel speed, and laser beam size on the melt pool geometry, has been studied. However, the effect of arc current on the melt pool geometry was not mentioned. In addition, how the heat source travel direction affects the melt pool geometry was not considered. More importantly, with a FE model, it is impossible to fully understand the effect of heat source travel direction on the melt pool geometry in the hybrid process. This is because the relative position between the two heat sources is changed with different travel directions, and this will affect the surface conditions and consequently the laser absorptivity. However, this could not be determined without an experimental examination, meaning that an experimental study is essential to reveal the effect of heat source travel direction on the melt pool geometry.

The aim of this study is to understand the response of melt pool geometry to different process parameters in the hybrid PTA-laser melting process. In this work, a parametric study of melt pool geometry was conducted with autogenous welding. The effect of different process parameters, including laser power, arc-laser separation distance, heat source travel direction, laser beam size, and arc current, on the melt pool geometry was revealed, and some recommendations were made for AM application. The results of this study will provide some fundamental information for the melt pool control in the hybrid arc-laser AM.

2 Experimental procedure

2.1 Materials and setup

The substrates used in the experiments were mild steel with the dimensions of 300 mm × 200 mm × 12 mm. The PTA was generated by a EWM power source, and pure argon was used for both plasma gas and shielding gas with a flowrate of 0.8 L/min and 8 L/min, respectively. An arc monitor (AMV 4000) was used to record the arc current and voltage. The laser beam was provided by a continuous wave fibre laser machine (IPG YLR-8000) with a maximum power of 8 kW. It should be mentioned that a defocused laser beam was used in all the studied cases. Figure 1a shows the experimental setup for the hybrid process. The plasma torch was inclined at an angle of 20° with respect to the travel direction to avoid any laser reflections, whilst the laser head was inclined at an angle of 30° perpendicular to the travel direction to avoid its back reflection. A process welding camera (Xiris XVC-1000) with a recording rate of 55fps and resolution of 1280 × 1024 was used to monitor the melt pool behaviour. The substrate was fixed with four clamps to prevent its movement. Figure 1b shows the configuration between the plasma torch, laser head, and substrate. In this study, the distance between the PTA and laser beam was defined as d, whilst the stand-off distance (h) of the plasma torch used was fixed at 8 mm. During the autogenous welding, the movement of the two heat sources was provided by a 6-axis Fanuc robot. The fixed parameters used for the two heat sources are shown in Table 1.

2.2 Methods

In this study, the response of the melt pool geometry to different process parameters, including laser power, arc-laser separation distance, travel direction, laser beam size, and arc current, was investigated. In total, 42 experimental cases were conducted, and the process parameters used for each

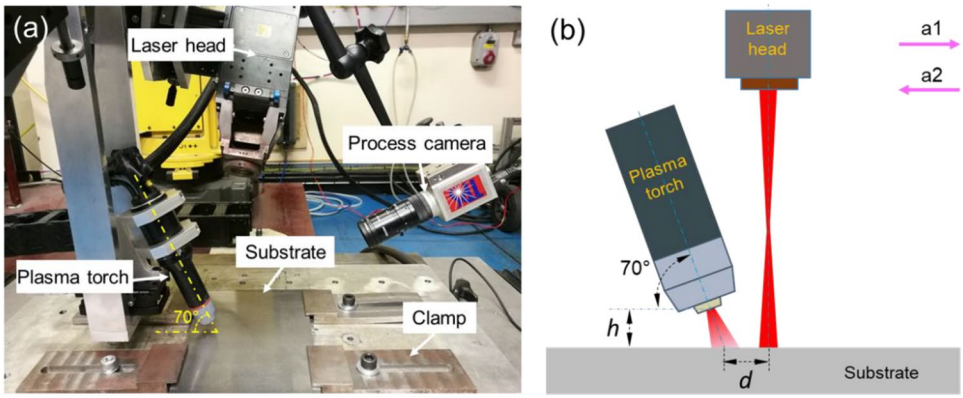

Fig. 1 **a** Experimental setup for the hybrid PTA-laser process and **b** the configuration for the two heat sources and substrate. Note, *a*1 and *a*2 represent the travel direction of laser-leading and arc-leading, respectively

Table 1 Fixed parameters used for the two heat sources

Heat source	Parameters (unit)	Value
PTA	Copper nozzle diameter (mm)	3.9
	Electrode diameter (mm)	4
	Angle of electrode tip (°)	40
	Set-back of electrode (mm)	2.4
	Copper nozzle to workpiece stand-off (mm)	8
	Plasma gas flowrate (L/min)	0.8
	Shielding gas flowrate (L/min)	8
	Angle of plasma torch (°)	20
Laser	Fibre diameter of the laser (mm)	0.3
	Focal length of the collimation lens (mm)	125
	Focal length of the focusing lens (mm)	250
	Focal spot diameter (mm)	0.6
	Angle of laser head (°)	30

case are shown in Table 2. To study the effect of a specific parameter on the melt pool geometry, this parameter was increased from a low value to a high value whilst keeping all the other parameters constant. For example, to study the laser power effect on the melt pool geometry, the laser power was increased from 0 to 5 kW with an interval of 1 kW whilst keeping other parameters constant (arc current of 160 A, arc-laser separation distance of 10 mm, laser beam diameter of 5 mm, travel speed of 5 mm/s, as shown in cases 1–12 in Table 2). Similarly, the effect of arc-laser separation distance was studied from cases 13–22 in Table 2. It should be mentioned that to study the abovementioned two effects, the experiments were conducted in both laser-leading and arc-leading travel directions. By doing this, the effect of heat source travel direction on the melt pool geometry can be examined by comparing cases 1–6 with cases 7–12, and by comparing cases 13–17 with cases 18–22. The effect of laser beam size on the melt pool geometry was studied with cases 23–32 in Table 2. In addition, some other cases (33–42) were conducted to study the effect of arc current on the melt pool geometry. In all the studied cases, the travel speed was kept constant at 5 mm/s, and the length of each autogenous welding bead was 120 mm. After autogenous welding, all the samples were cross-sectioned, hot mounted, ground, polished, and etched (using 4% Nital) to check the fusion zone and heat-affected zone (HAZ), and images were taken using a Nikon stereo microscope.

3 Results and discussion

3.1 Effect of laser power

Figure 2 shows the effect of laser power on the melting process and fusion zone in both laser-leading and PTA-leading travel directions. In both scenarios, the melt pool became wider and deeper with the increase of laser power, evident as the increased width and depth of fusion zone. Also, the images captured by the process camera show that two separated melt pools were formed at a relatively low laser power, and they merged into one big common melt pool as the laser power increased to a high value.

Figure 3 shows the dimensions of the corresponding fusion zones as described in Fig. 2. The increased melt pool size was attributed to the increased energy input. As shown in Fig. 3a, the melt pool width almost doubled (from 4.0 to 7.2 mm) as the laser power increased from 0 to 5 kW with a laser-leading travel direction. Also, it can be seen from Fig. 3b that the melt pool depth increased significantly from 0.2 to 4.0 mm as the laser power increased from 0 to 5 kW with an arc-leading travel direction. In addition, by comparing the cross-sectional area of the fusion zone in Fig. 2a and b, different material responses were observed with the two different heat source travel directions, which will be discussed in Sect. 3.3.

3.2 Effect of arc-laser separation distance

Figure 4 shows the effect of arc-laser separation distance on the melting process and fusion zone in two travel directions.

Table 2 Process parameters used to study the effect of each parameter on the melt pool geometry

Parametric study	Case	Arc current (A)	Arc voltage (V)	Laser power (kW)	Arc-laser distance (mm)	Laser beam diameter (mm)	Travel direction	Travel speed (mm/s)
Laser power	1	160	22.4	0	10	5	*a*1	5
	2	160	22.4	1	10	5	*a*1	5
	3	160	22.4	2	10	5	*a*1	5
	4	160	22.4	3	10	5	*a*1	5
	5	160	22.4	4	10	5	*a*1	5
	6	160	22.4	5	10	5	*a*1	5
	7	160	22.4	0	10	5	*a*2	5
	8	160	22.4	1	10	5	*a*2	5
	9	160	22.4	2	10	5	*a*2	5
	10	160	22.4	3	10	5	*a*2	5
	11	160	22.4	4	10	5	*a*2	5
	12	160	22.4	5	10	5	*a*2	5
Arc-laser separation distance	13	160	22.4	3	6	5	*a*1	5
	14	160	22.4	3	8	5	*a*1	5
	15	160	22.4	3	10	5	*a*1	5
	16	160	22.4	3	12	5	*a*1	5
	17	160	22.4	3	14	5	*a*1	5
	18	160	22.4	3	6	5	*a*2	5
	19	160	22.4	3	8	5	*a*2	5
	20	160	22.4	3	10	5	*a*2	5
	21	160	22.4	3	12	5	*a*2	5
	22	160	22.4	3	14	5	*a*2	5
Laser beam size	23	160	22.4	3	10	6	*a*2	5
	24	160	22.4	3	10	7	*a*2	5
	25	160	22.4	3	10	8	*a*2	5
	26	160	22.4	3	10	9	*a*2	5
	27	160	22.4	3	10	10	*a*2	5
	28	160	22.4	1	10	10	*a*2	5
	29	160	22.4	2	10	10	*a*2	5
	30	160	22.4	3	10	10	*a*2	5
	31	160	22.4	4	10	10	*a*2	5
	32	160	22.4	5	10	10	*a*2	5
Arc current	33	200	25.8	1	10	10	*a*2	5
	34	200	25.8	2	10	10	*a*2	5
	35	200	25.8	3	10	10	*a*2	5
	36	200	25.8	4	10	10	*a*2	5
	37	200	25.8	5	10	10	*a*2	5
	38	0	0	5	10	5	*a*1	5
	39	120	18.9	5	10	5	*a*1	5
	40	160	22.4	5	10	5	*a*1	5
	41	200	25.8	5	10	5	*a*1	5
	42	250	29.8	5	10	5	*a*1	5

During the melting process, a short arc-laser separation distance resulted in a common melt pool, whilst a relatively long separation distance resulted in two separated melt pools. For example, with a laser-leading travel direction, a common melt pool was observed with a separation distance of 6 mm and 10 mm, whilst two separated melt pools were observed with a separation distance of 14 mm (Fig. 4a). However, for a given travel direction, the melt pool geometry

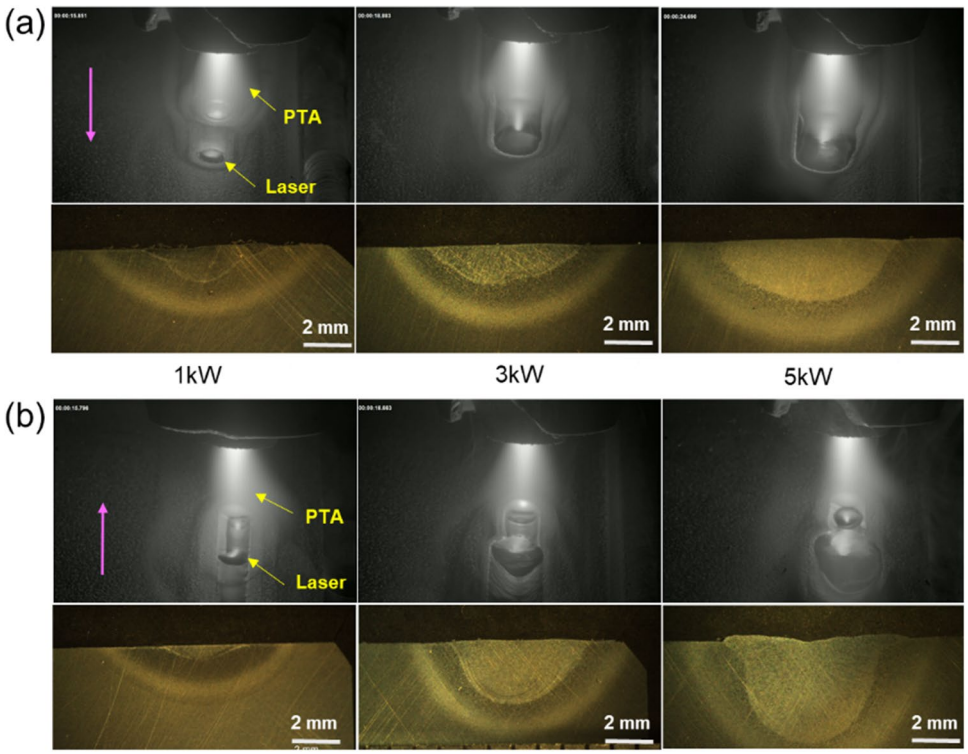

Fig. 2 The effect of laser power on the melting process and melt pool geometry at different travel directions: **a** laser-leading and **b** PTA-leading. Pink arrow indicates the heat source travel direction. All the process parameters used are shown in cases (2, 4, 6, 8, 10, 12) of Table 2

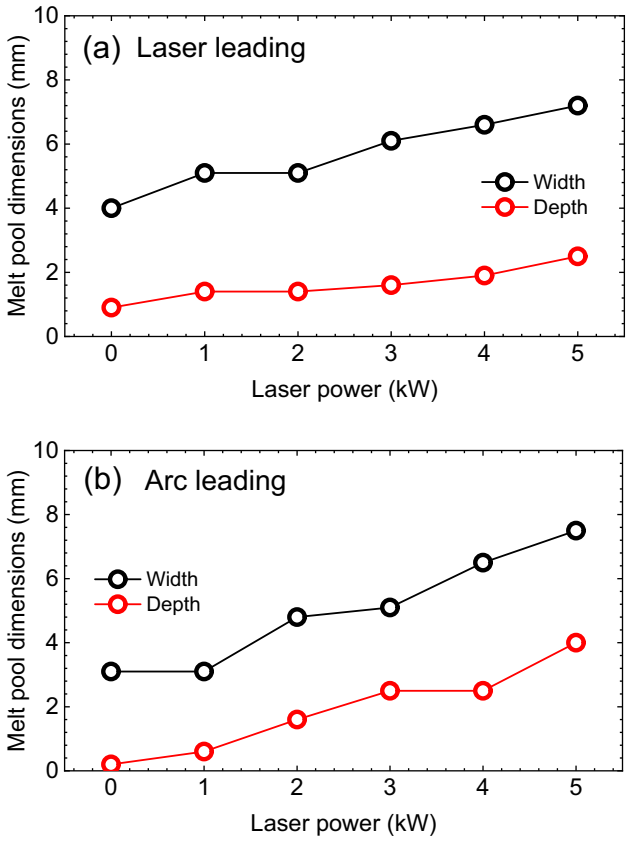

Fig. 3 The effect of laser power on the melt pool geometry at different travel directions: **a** laser-leading and **b** PTA-leading. All the process parameters used are shown in cases 1–12 of Table 2

did not change significantly with the increase of separation distance.

Figure 5 shows the melt pool dimensions of the corresponding cases as described in Fig. 4. In Fig. 5a, with a laser-leading travel direction, the melt pool width reduced slightly from 6.6 to 5.2 mm whilst the melt pool depth was almost unchanged at a value of 1.8 mm as the separation distance increased from 6 to 14 mm. Similarly, with a PTA-leading travel direction, the melt pool width reduced slightly from 7.0 to 5.9 mm whilst the melt pool depth reduced slightly from 3 to 2.4 mm as the separation distance increased from 6 to 14 mm (Fig. 5b). The minor difference in melt pool dimensions was attributed to the unchanged total energy input in the studied cases. Although the melt pool geometry did not change significantly with the selected range of arc-laser separation distance, a continuous melt pool is desirable in AM process to achieve a bead with high quality [9]. It is similar as described in Sect. 3.1, the heat source travel direction also affects the melt pool geometry in these cases. This can be known by comparing the cross-sectional area of the fusion zone shown in Fig. 4a and b, and the effect of travel direction will be discussed in the next section.

3.3 Effect of travel direction

As shown in both Figs. 2 and 4, for the same process parameters used, the melt pool geometry achieved with laser-leading and PTA-leading travel directions was different.

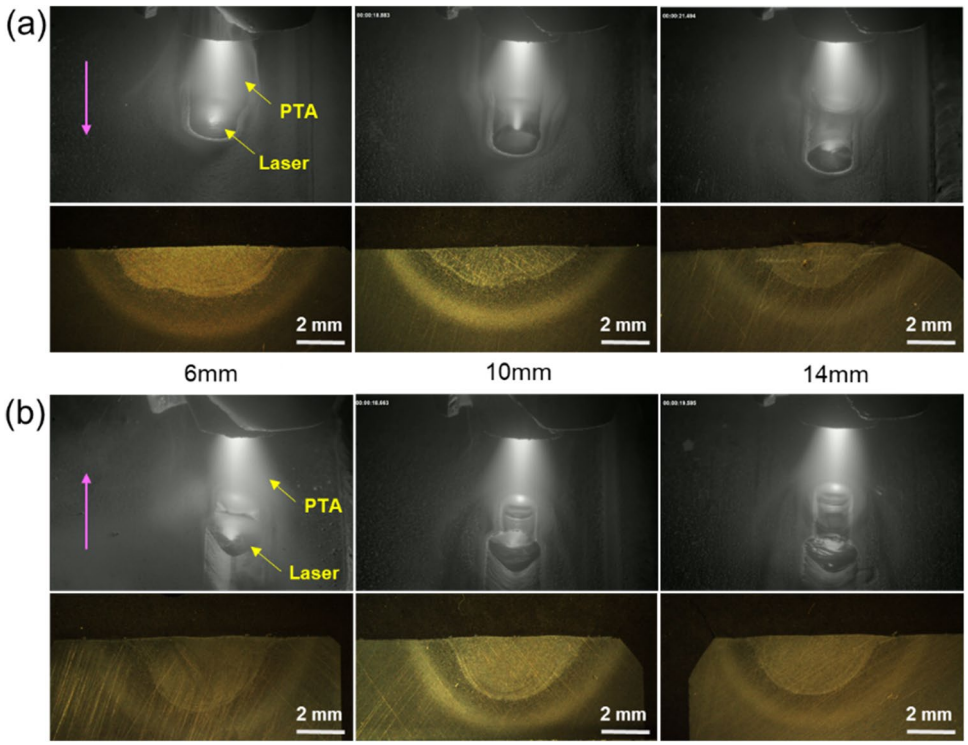

Fig. 4 The effect of arc-laser separation distance on the melting process and melt pool geometry at different travel directions: **a** laser-leading and **b** PTA-leading. All the process parameters used are shown in cases (13, 15, 17, 18, 20, 22) of Table 2

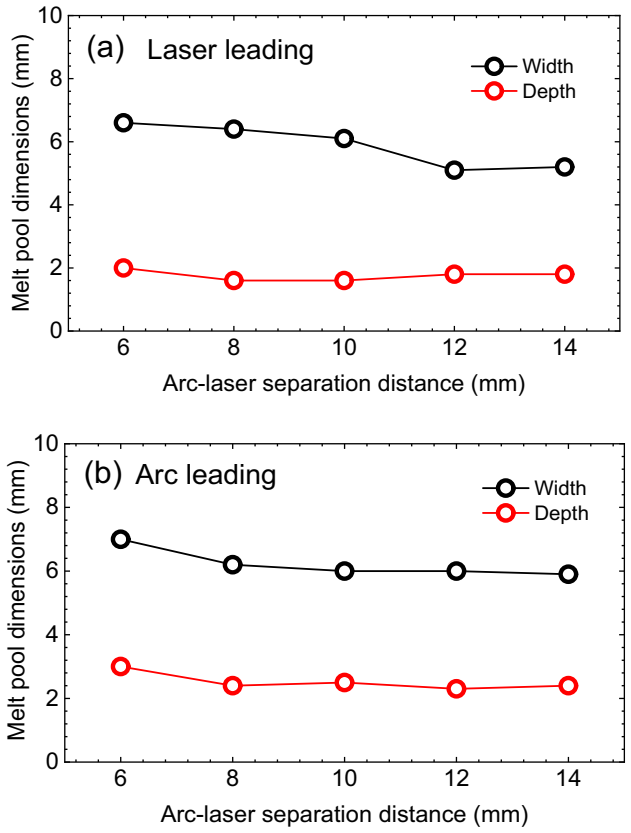

Fig. 5 The effect of arc-laser separation distance on the melt pool geometry at different travel directions: **a** laser-leading and **b** PTA-leading. All the process parameters used are shown in cases 13–22 of Table 2

More specifically, a deeper melt pool was achieved with the PTA-leading travel direction compared to that with the laser-leading travel direction. Figure 6 shows the cross-sectional area of the fusion zones as described in Figs. 3 and 5. One can see that a larger cross-sectional area is always achieved with the PTA-leading travel direction (except the first case in Fig. 6a), indicating that more energy was absorbed by the workpiece with this travel direction.

In this study, the only difference with two different travel directions is the relative position between the two heat sources. In the laser-leading travel direction, the laser was at the front of the PTA and pointed to a substrate with room temperature, whilst in the PTA-leading travel direction, the laser was at the back of the PTA and reached a pre-heated substrate or already melted material caused by the PTA. It is well known that laser absorptivity varies significantly depending on the process regime, material type, and its surface conditions and processing conditions [24–27]. Among these, it was reported that laser absorptivity is significantly affected by the workpiece temperature [28]. Normally, the higher the workpiece temperature, the higher the laser absorptivity. Also, there is a significant increase in laser absorptivity when the material is heated to melting temperature [29]. This means that in the hybrid process, the laser absorptivity is higher with the PTA-leading travel direction compared to that with the laser-leading travel direction due to a higher workpiece temperature occurred in the former case, leading to a higher energy input with the former travel direction. As a result, a bigger melt pool was formed with

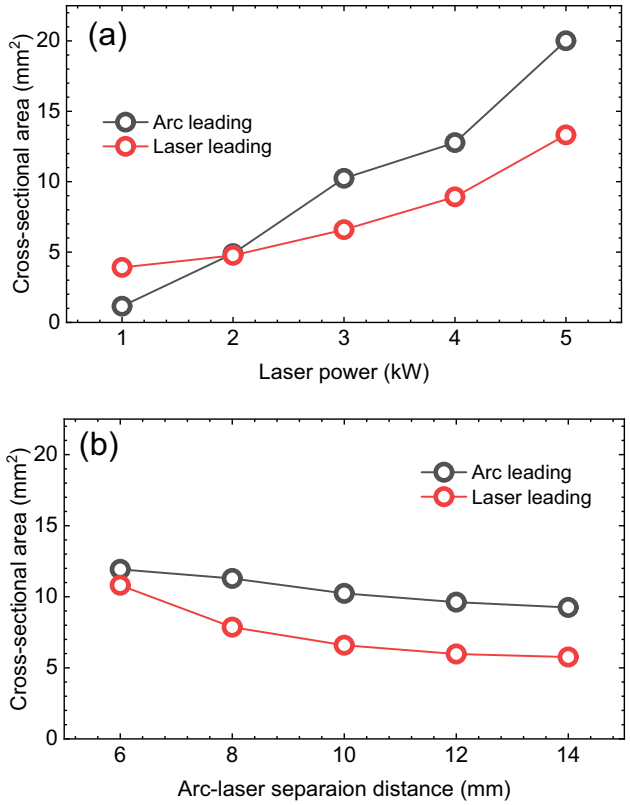

Fig. 6 Cross-sectional area of the fusion zone obtained with different travel directions at different **a** laser power and **b** arc-laser separation distance. All the process parameters used are shown in cases (2–6, 8–22) of Table 2

the PTA-leading travel direction than that with the laser-leading travel direction. This suggests that in AM process, a higher thermal efficiency and thus a higher deposition rate will be achieved with the arc-leading configuration.

3.4 Effect of laser beam size

Figure 7 shows the melt pool dimensions as a function of laser beam diameter at the same arc current and laser power, and Fig. 8 shows the cross-section of two typical

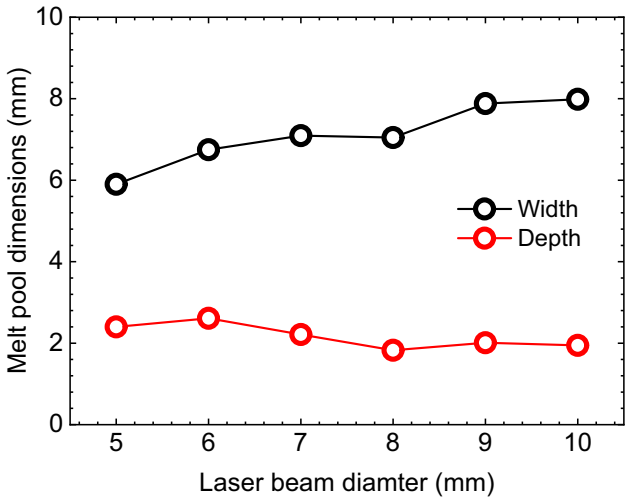

Fig. 7 The effect of laser beam size on the melt pool geometry. All the process parameters used are shown in cases (10, 23–27) of Table 2

cases described in Fig. 7. It can be seen from both Figs. 7 and 8 that a wider and shallower melt pool was formed with a larger laser beam at the same total energy input. It was reported that the laser beam size did not have a significant effect on the melt pool size and geometry in the hybrid PTA-laser AM [10]. This is because in that case, the laser beam was much smaller than the melt pool width, where the melt pool width was dominant by the melt flow. Here, however, the laser beam was bigger than the melt pool, and the melt pool width is dependent on the laser beam size.

Some other cases were conducted to compare the laser size effect at different laser powers, and the cross-sections of the samples are shown in Fig. 9. For a given laser power, a deeper and narrower bead (i.e. lower width-to-depth ratio) was achieved with a smaller laser beam. It was reported that in conduction laser welding, the penetration depth is proportional to the power density and interaction time [30]. For a circular laser beam, the power density, E, is expressed by:

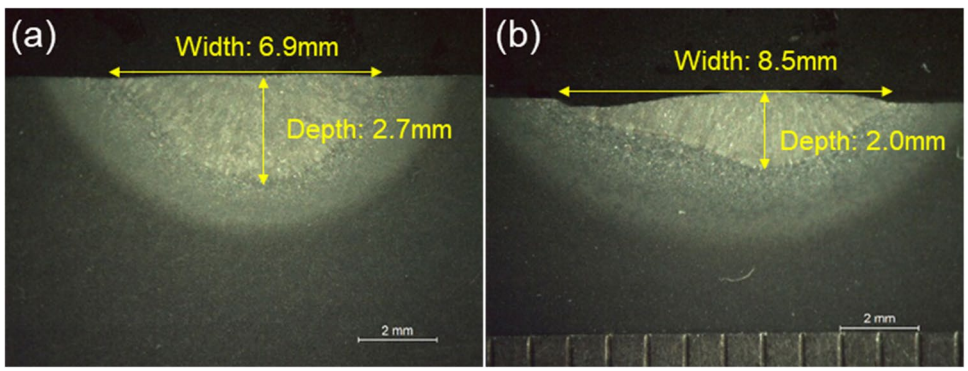

Fig. 8 Fusion zone obtained with different laser beam diameters: **a** 6 mm and **b** 10 mm. All the process parameters used are shown in cases (23, 27) of Table 2

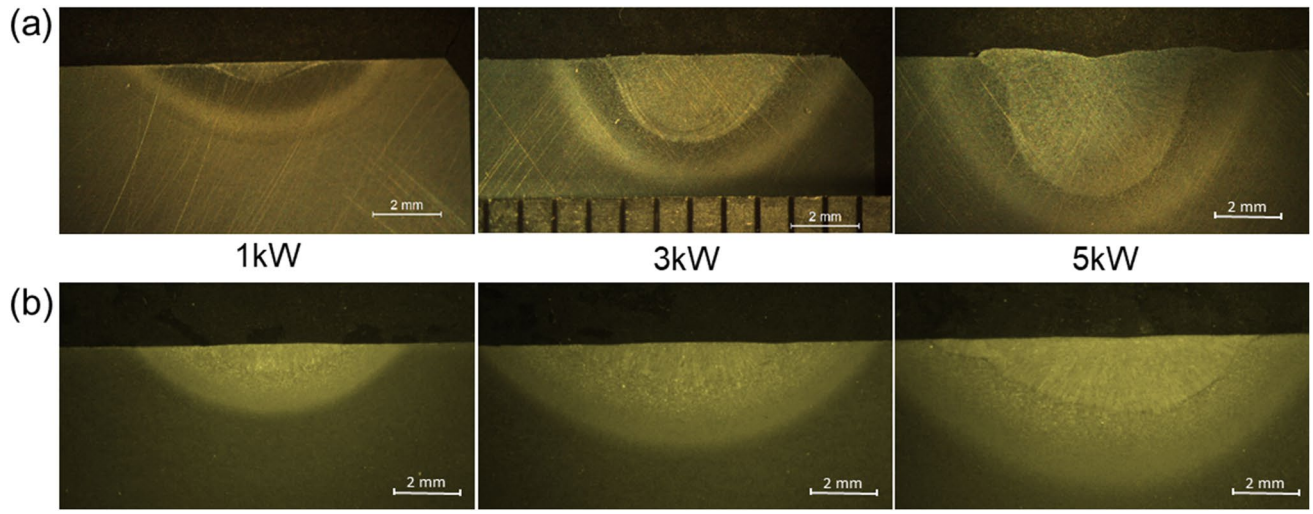

Fig. 9 Fusion zone obtained at different laser powers with a laser beam diameter of: **a** 5 mm and **b** 10 mm. All the process parameters used are shown in cases (8, 10, 12, 28, 30, 32) of Table 2

$$E = \frac{4P}{\pi d^2} \tag{1}$$

where P is the laser power, and d is the laser beam diameter. The interaction time, t_i, is defined as the ratio of laser beam diameter to its travel speed, which is given by:

$$t_i = \frac{d}{v} \tag{2}$$

where v is laser travel speed. From Eq. (1), the power density reduces quadratically with the laser beam diameter, and from Eq. (2), one can see that the interaction time increases linearly with the laser diameter. The travel speed was fixed in this study. Therefore, the penetration depth reduces whilst the width increases with the increasing laser beam size.

3.5 Effect of current

Figure 10 shows the comparison of melt pool dimensions at two different levels of arc current with the PTA-leading configuration, and Fig. 11 shows the cross-section of some cases as described in Fig. 10. From both Figs. 10 and 11, for a given laser power, a wider and deeper melt pool was always achieved with a current of 200 A compared to that with a current of 160 A. Also, for a given arc current, both the melt pool width and depth increase with the increase of laser power. In these cases, a large laser beam diameter of 10 mm was used. Chen et al. [31] used a split anode calorimetry to measure the PTA energy density and found that the diameter of a PTA is around 14 mm. In addition, the output powers for an arc current of 160 A and 200 A are around 3.5 kW and 5 kW, respectively. This means that the power densities for the PTA and laser are comparable, and neither of them

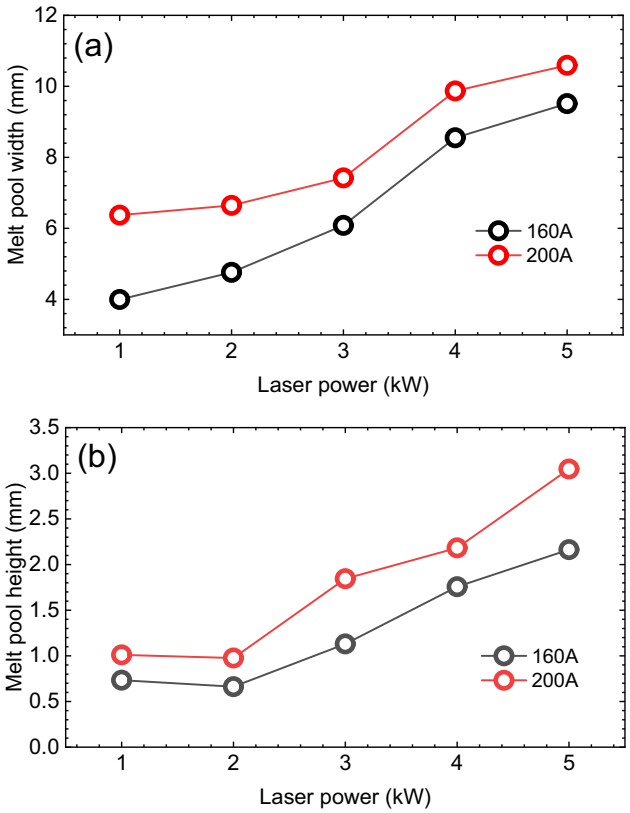

Fig. 10 The effect of arc current on melt pool dimensions with the PTA-leading configuration. An arc-laser separation distance of 10 mm and laser beam diameter of 10 mm were used in these cases. All the process parameters used are shown in cases 28–37 of Table 2

is dominant in controlling the melt pool depth. Therefore, both the melt pool depth and width are sensitive to both arc current and laser power in these cases.

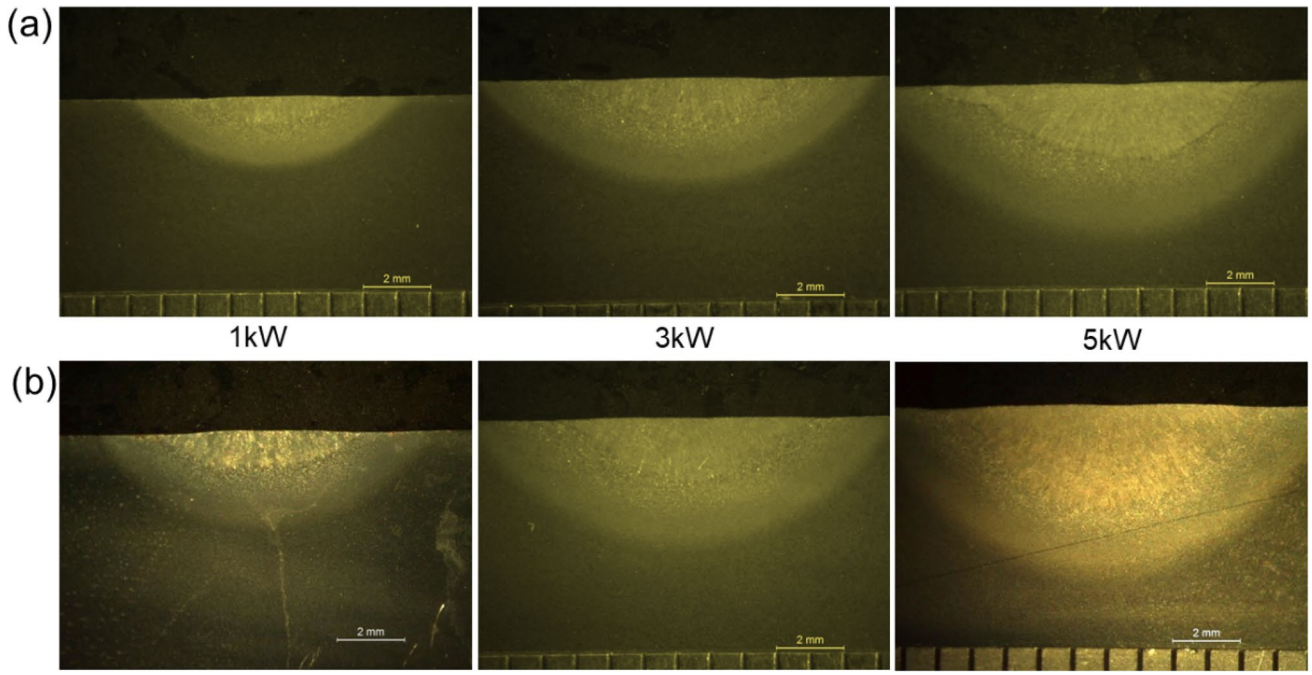

Fig. 11 The effect of arc current on melt pool dimensions: **a** 160 A and **b** 200 A. All the process parameters used are shown in cases (28, 30, 32, 33, 35, 37) of Table 2

Figure 12 shows the effect of the arc current on the melt pool geometry with the laser-leading configuration, and Fig. 13 shows the corresponding melting process and cross-section. From Fig. 12, the melt pool width increases proportionally as the arc current increases from 120 to 250 A,

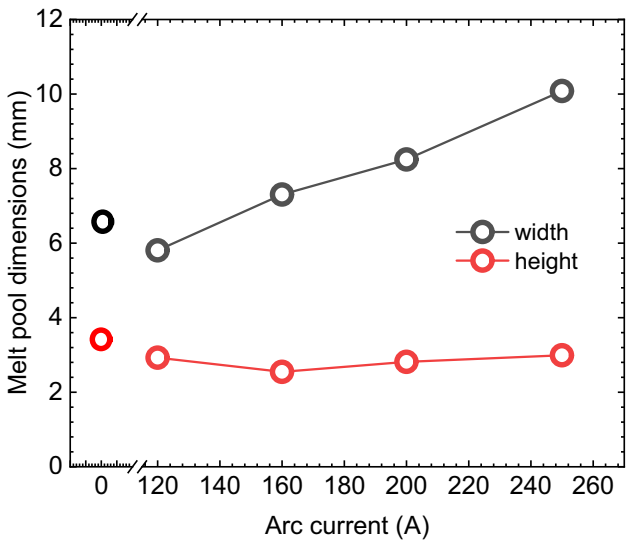

Fig. 12 The effect of arc current on melt pool dimensions with the laser-leading configuration. A separation distance of 10 mm, laser beam diameter of 5 mm, and laser power of 5 kW were used in these cases. All the process parameters used are shown in cases 38–42 of Table 2

but the melt pool depth was almost unchanged at 2.8 mm. It should be mentioned that a relatively small laser beam diameter of 5 mm and a high laser power of 5 kW were used in these cases. This means that the power density of laser is much larger than that of PTA. Therefore, the melt pool depth was determined by the laser. This also can be proven by Fig. 13b, where the melt pool depth with a laser-only process (i.e. no arc) is even slightly larger than those with the hybrid arc-laser process. Figure 14 shows the PTA-only process at a current of 160 A, where a very shallow melt pool was formed with a depth of 0.2 mm. In addition, a large heat-affected zone (HAZ) was observed in this case, indicating that the power density of the PTA is relatively low. The large PTA beam and relatively low power density promoted the melt pool spreading in the transverse direction and consequently increased the melt pool width.

The control of the melt pool geometry by manipulating different process parameters in the hybrid PTA-laser process was studied systematically. Overall, compared to the arc-laser separation distance, the melt pool geometry is more sensitive to laser beam size, laser power, and arc current. Normally, in arc-based processes, both the melt pool width and depth increase with the increase of arc current [32, 33]. However, in the hybrid arc-laser process, this not only depends on the energy input of the arc and laser but also depends on their power density. In addition, with different heat source configurations (or travel directions), the energy absorbed by the workpiece is different, and the PTA-leading

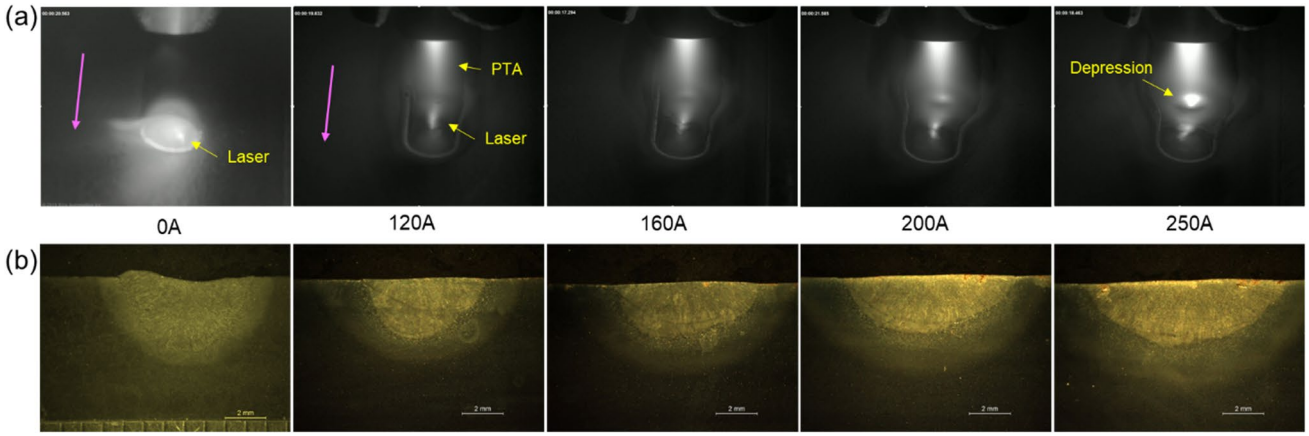

Fig. 13 The effect of the current on the **a** melting process and **b** cross-section in the hybrid PTA-laser process. All the parameters used are shown in cases 38–42 of Table 2

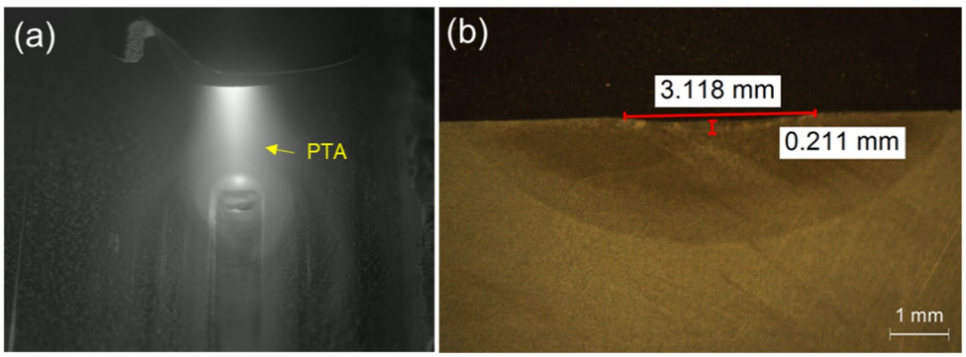

Fig. 14 **a** The melting process and **b** the cross-section of the resultant bead, for a PTA-only process at an arc current of 160 A. All the process parameters used are shown in case 7 of Table 2

configuration is preferred in the hybrid AM to achieve a higher process efficiency. All these results obtained from this study can provide useful information for the hybrid arc-laser AM process.

4 Conclusions

1. In both laser-leading and PTA-leading configurations, both the melt pool width and depth increase with the increase of laser power due to the increased energy input.
2. The arc-laser separation distance did not have a significant effect on the melt pool width and depth due to the unchanged energy input, but a short separation distance is desirable to avoid two separated melt pools.
3. A larger melt pool was achieved with the PTA-leading travel direction compared to that with the laser-leading travel direction. This is because more energy was received by the workpiece with the former travel direction due to the higher laser absorptivity occurred in this case.
4. A bigger laser beam diameter promotes a shallower and wider melt pool. When the laser beam is bigger than the melt pool width, the melt pool width is determined by the laser beam size.
5. The melt pool became wider and deeper with the increase of arc current, provided that the arc power density and laser power density are comparable. The melt pool became wider, but the depth did not change significantly with the increase of arc current with a laser-leading configuration. This was caused by the high laser power density, which determined the melt pool depth.

Acknowledgements The authors also would like to thank John Thrower, Nielsen Flemming, Nisar Shah, and Steve Pope for the technical assistance.

Funding The authors would like to thank Engineering and Physical Sciences Research Council (EPSRC) for the financial support of this research (NEWAM: EP/R027218/1).

Data Availability Data underlying this study can be accessed through the Cranfield University repository at https://doi.org/10.17862/cranfield.rd.21923409.

Declarations

Conflict of interest The authors declare no competing interests.

References

1. Chen G, Williams S, Ding J, et al (2022) Multi-energy source (MES) configuration for bead shape control in wire-based directed energy deposition (w-DED). J Mater Process Technol 304:. https://doi.org/10.1016/j.jmatprotec.2022.117549
2. DebRoy T, Wei HL, Zuback JS et al (2018) Additive manufacturing of metallic components – process, structure and properties. Prog Mater Sci 92:112–224. https://doi.org/10.1016/j.pmatsci.2017.10.001
3. Chen X, Wang C, Ding J et al (2022) A three-dimensional wire-feeding model for heat and metal transfer, fluid flow, and bead shape in wire plasma arc additive manufacturing. J Manuf Process 83:300–312. https://doi.org/10.1016/j.jmapro.2022.09.012
4. Liverani E, Toschi S, Ceschini L, Fortunato A (2017) Effect of selective laser melting (SLM) process parameters on microstructure and mechanical properties of 316L austenitic stainless steel. J Mater Process Technol 249:255–263. https://doi.org/10.1016/j.jmatprotec.2017.05.042
5. Galati M, Iuliano L (2018) A literature review of powder-based electron beam melting focusing on numerical simulations. Addit Manuf 19:1–20. https://doi.org/10.1016/j.addma.2017.11.001
6. Williams SW, Martina F, Addison AC et al (2016) Wire + Arc additive manufacturing. Mater Sci Technol (United Kingdom) 32:641–647. https://doi.org/10.1179/1743284715Y.0000000073
7. Ding D, Pan Z, Cuiuri D, Li H (2015) Wire-feed additive manufacturing of metal components: technologies, developments and future interests. Int J Adv Manuf Technol 81:465–481. https://doi.org/10.1007/s00170-015-7077-3
8. Fayazfar H, Salarian M, Rogalsky A et al (2018) A critical review of powder-based additive manufacturing of ferrous alloys: process parameters, microstructure and mechanical properties. Mater Des 144:98–128. https://doi.org/10.1016/j.matdes.2018.02.018
9. Wang C, Suder W, Ding J, Williams S (2021) Wire based plasma arc and laser hybrid additive manufacture of Ti-6Al-4V. J Mater Process Technol 293:117080. https://doi.org/10.1016/j.jmatprotec.2021.117080
10. Wang C, Suder W, Ding J, Williams S (2021) Bead shape control in wire based plasma arc and laser hybrid additive manufacture of Ti-6Al-4V. J Manuf Process 68:1849–1859. https://doi.org/10.1016/j.jmapro.2021.07.009
11. Wang C, Sun Y, Chen G, et al (2022) A simplified modelling approach for thermal behaviour analysis in hybrid plasma arc-laser additive manufacturing. Int J Heat Mass Transf 195:. https://doi.org/10.1016/j.ijheatmasstransfer.2022.123157
12. Acherjee B (2018) Hybrid laser arc welding: state-of-art review. Opt Laser Technol 99:60–71. https://doi.org/10.1016/j.optlastec.2017.09.038
13. Shi J, Song G, Wang H, Liu L (2018) Study on weld formation and its mechanism in laser-TIG hybrid welding with filler wire of a titanium alloy. J Laser Appl 30:032004. https://doi.org/10.2351/1.5042205
14. Chen YB, Lei ZL, Li LQ, Wu L (2006) Experimental study on welding characteristics of CO2 laser TIG hybrid welding process. Sci Technol Weld Join 11:403–411. https://doi.org/10.1179/174329306X129535
15. Zhang C, Gao M, Wang D et al (2017) Relationship between pool characteristic and weld porosity in laser arc hybrid welding of AA6082 aluminum alloy. J Mater Process Technol 240:217–222. https://doi.org/10.1016/j.jmatprotec.2016.10.001
16. Liu S, Liu F, Zhang H, Shi Y (2012) Analysis of droplet transfer mode and forming process of weld bead in CO 2 laserMAG hybrid welding process. Opt Laser Technol 44:1019–1025. https://doi.org/10.1016/j.optlastec.2011.10.016
17. Shenghai Z, Yifu S, Huijuan Q (2013) The technology and welding joint properties of hybrid laser-tig welding on thick plate. Opt Laser Technol 48:381–388. https://doi.org/10.1016/j.optlastec.2012.11.014
18. Le Guen E, Fabbro R, Carin M et al (2011) Analysis of hybrid Nd: Yag laser-MAG arc welding processes. Opt Laser Technol 43:1155–1166. https://doi.org/10.1016/j.optlastec.2011.03.002
19. Zhang LJ, Ning J, Zhang XJ et al (2015) Single pass hybrid laser-MIG welding of 4-mm thick copper without preheating. Mater Des 74:1–18. https://doi.org/10.1016/j.matdes.2015.02.027
20. Bidi L, Mattei S, Cicala E et al (2011) The use of exploratory experimental designs combined with thermal numerical modelling to obtain a predictive tool for hybrid laser/MIG welding and coating processes. Opt Laser Technol 43:537–545. https://doi.org/10.1016/j.optlastec.2010.07.011
21. Chen X, Mu Z, Hu R et al (2019) A unified model for coupling mesoscopic dynamics of keyhole, metal vapor, arc plasma, and weld pool in laser-arc hybrid welding. J Manuf Process 41:119–134. https://doi.org/10.1016/j.jmapro.2019.03.034
22. Wang C, Suder W, Ding J, Williams S (2021) The effect of wire size on high deposition rate wire and plasma arc additive manufacture of Ti-6Al-4V. J Mater Process Technol 288:116842. https://doi.org/10.1016/j.jmatprotec.2020.116842
23. Pardal G, Martina F, Williams S (2019) Laser stabilization of GMAW additive manufacturing of Ti-6Al-4V components. J Mater Process Technol 272:1–8. https://doi.org/10.1016/j.jmatprotec.2019.04.036
24. Bunaziv I, Akselsen OM, Ren X et al (2021) Laser beam and laser-arc hybrid welding of aluminium alloys. Met 11:1150. https://doi.org/10.3390/MET11081150

25. Nath AK, Sridhar R, Ganesh P, Kaul R (2002) Laser power coupling efficiency in conduction and keyhole welding of austenitic stainless steel. Sadhana - Acad Proc Eng Sci 27:383–392. https://doi.org/10.1007/BF02703659
26. Indhu R, Vivek V, Sarathkumar L et al (2018) Overview of laser absorptivity measurement techniques for material processing. Lasers Manuf Mater Process 5:458–481. https://doi.org/10.1007/s40516-018-0075-1
27. Fuerschbach PW, MacCallum DO (2018) Variation of laser energy transfer efficiency with weld pool depth 497:497–503. https://doi.org/10.2351/1.5058947
28. Kwon H, Baek WK, Kim MS et al (2012) Temperature-dependent absorptance of painted aluminum, stainless steel 304, and titanium for 1.07 μm and 10.6 μm laser beams. Opt Lasers Eng 50:114–121. https://doi.org/10.1016/j.optlaseng.2011.10.001
29 Khaskin VY, Korzhik VN, Chizhskaya TG et al (2016) Effect of laser radiation absorption on efficiency of laser welding of copper and its alloys. Paton Weld J 2016:35–39. https://doi.org/10.15407/as2016.11.05
30. Ayoola WA, Suder WJ, Williams SW (2017) Parameters controlling weld bead profile in conduction laser welding. J Mater Process Technol 249:522–530. https://doi.org/10.1016/j.jmatprotec.2017.06.026
31. Chen G, Williams S, Ding J et al (2022) Split anode calorimetry for plasma arc energy density measurement with laser calibration. J Manuf Process 78:71–81. https://doi.org/10.1016/j.jmapro.2022.04.003
32. Martina F, Mehnen J, Williams SW et al (2012) Investigation of the benefits of plasma deposition for the additive layer manufacture of Ti-6Al-4V. J Mater Process Technol 212:1377–1386. https://doi.org/10.1016/j.jmatprotec.2012.02.002
33. Dinovitzer M, Chen X, Laliberte J et al (2019) Effect of wire and arc additive manufacturing (WAAM) process parameters on bead geometry and microstructure. Addit Manuf 26:138–146. https://doi.org/10.1016/j.addma.2018.12.013